Dalton Transactions

ROYAL SOCIETY OF CHEMISTRY

PAPER

View Article Online
View Journal | View Issue

Cite this: *Dalton Trans.*, 2024, **53**, 2231

Well-defined Cu(I) complexes based on [N,P]-pyrrole ligands catalyzed a highly endoselective 1,3-dipolar cycloaddition†

Miguel A. Alvarado-Castillo,[a,b] Salvador Cortés-Mendoza,[a] José E. Barquera-Lozada,[a] Francisco Delgado,*[b] Ruben A. Toscano,[a] M. Carmen Ortega-Alfaro[c] and José G. López-Cortés*[a]

Received 4th November 2023,
Accepted 20th December 2023

DOI: 10.1039/d3dt03692h

rsc.li/dalton

We herein report the synthesis and catalytic application of a new family of dinuclear Cu(I) complexes based on [N,P]-pyrrole ligands. The Cu(I) complexes (**4a–d**) were obtained in good yields and their catalytic properties were evaluated in the1,3-dipolar cycloaddition of azomethine ylides and electron-deficient alkenes. The air-stable complexes **4a–d** exhibited high endo-diasteroselectivity to obtain substituted pyrrolidines, and the catalytic system showed excellent reactivity and wide substitution tolerance.

Introduction

Nowadays, copper(I) complexes have acquired great importance in the design of new materials for organic light-emitting devices (OLEDs)[1] and photosensitizers.[2] Likewise, the catalytic properties of these complexes have been largely explored. In the literature, we can find some recent examples of using Cu(I) in combination with [N,P] ligands in important catalytic transformations. These included conjugated additions of boron to α,β-unsaturated compounds,[3] asymmetric alkylation of indoles,[4] direct asymmetric alkynylation of α-ketoesters,[5] and asymmetric A3 couplings,[6] among others. Particularly, the 1,3-dipolar cycloaddition (1,3-DC) of azomethine ylides to electron-deficient alkenes constitutes one of the most powerful and versatile methods to obtain highly substituted 5-membered heterocycles.[7,8] This reaction can be accomplished using several metal complexes such as zinc(II),[9] nickel(II),[10] silver(I),[11] copper(I),[12] and copper(II).[13] Particularly, in the case of copper (I) catalyzed reactions, the use of hemilabile ferrocenyl [N,P]-ligands appears as an interesting approach that allows the synthesis of *exo*-aducts[12b] with good to excellent diastereo- and enantio-selective results. On the other hand, the synthesis of *endo*-adducts is favored when [N,N]-, [S,S]- and [P,S]-ligands are used in combination with different sources of copper(I) precursors.[12j–m] Similar results were obtained with the catalytic systems of Zn(II)/N,O-ligands[9a] and Ag(I)/chiral BINOL-derived phosphoric acids.[11d]

Previously, we reported an efficient synthesis of pyrrole-based [N,P] ligands with a dimethylamine group and a phosphine moiety as hard and soft donors, respectively.[14] Moreover, we have demonstrated that their palladium complexes catalyzed some C–C coupling reactions,[15] their gold(I)-complexes catalyzed the cycloisomerization of enynes,[16] and their ruthenium counterparts promoted the transfer hydrogenation of ketones (Fig. 1).[17] As part of our continuous interest in developing catalytic applications of [N,P]-pyrrole phosphines, in this work we address the synthesis of new copper(I)-[N,P] dinuclear complexes, which were tested in 1,3-dipolar cycloaddition, obtaining pyrrolidines with high endo-selectivity.

Results and discussion

Initially, we synthesized the ligands **2a–d** in good yields using the methodology previously described by our group.[14,15] In order to know about the σ-donor behavior of these phosphines, we reacted **2a–d** with elemental selenium overnight in an NMR tube at 0 °C using $CDCl_3$ as the solvent (Scheme 1).

Thereafter, we obtained $^{31}P\{^1H\}$ NMR spectra. The values obtained for the coupling constant J_{P-Se} are shown in Table 1. In general, all phosphine selenides with an alkyl group (Table 1, entries 2–4) exhibit lower J_{P-Se} values compared to

[a]*Instituto de Química, Universidad Nacional Autónoma de México, Circuito Exterior, Ciudad Universitaria, Coyoacán, C.P. 04360 CdMx, Mexico. E-mail: jglcvdw@unam.mx*
[b]*Departamento de Química Organica, Escuela Nacional de Ciencias Biológicas Instituto Politécnico Nacional Prol. Carpio y Plan de Ayala, S/N, CdMx, 11340, Mexico*
[c]*Instituto de Ciencias Nucleares, Universidad Nacional Autónoma de México, Circuito Exterior, Ciudad Universitaria, Coyoacán, C.P. 04510 CdMx, Mexico*

†Electronic supplementary information (ESI) available: Experimental procedures and characterization data of all compounds. CCDC 2295705–2295708 (**4a–b**). For ESI and crystallographic data in CIF or other electronic format see DOI: https://doi.org/10.1039/d3dt03692h

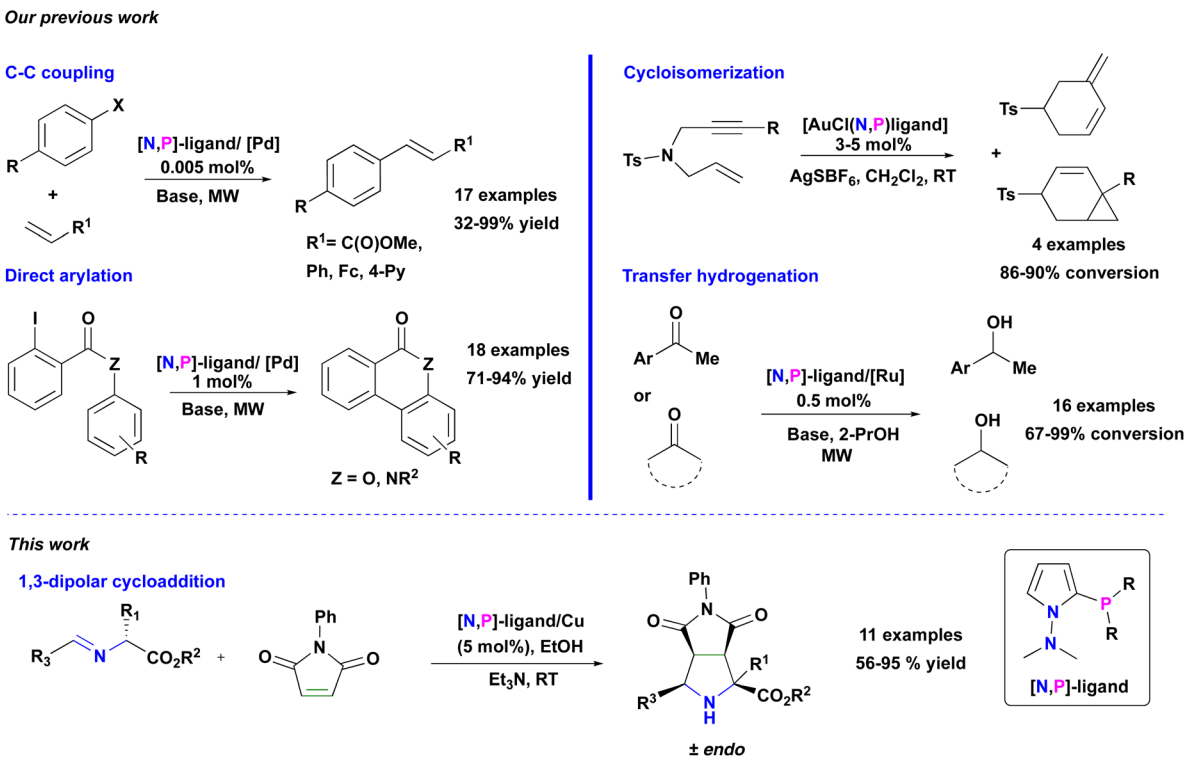

Fig. 1 Catalytic applications of [N,P] ligands based on pyrrole.

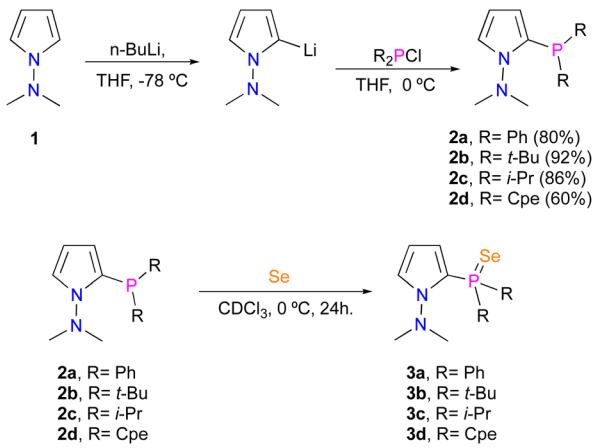

Scheme 1 Preparative route to [N,P] ligands based on pyrrole **2a–d**.

Table 1 ^{31}P NMR chemical shift for [N,P] ligands based on pyrrole and their selenides analogues[a]

Entry	Phosphine	R	$\delta^{31}P_{ligand}$ [b]	$\delta^{31}P_{P-Se}$ [b]	$^{1}J_{P-Se}$ [c]
1	**2a**[15]	Ph	−29.2	16.2	736
2	**2b**[14]	*t*-Bu	1.5	72.4[d]	707
3	**2c**[15]	i-Pr	−17.6	56.4	704
4	**2d**[16]	*c*Pent	−25.6	50.2	705
5	PPh_3[18]	—	−4.7	35.2	730
6	*t*-Bu_3P[18]	—	61.1	92.9	687
7	i-Pr_3P[18]	—	19	70.5	686
8	*c*$Pent_3P$[18]	—	4.7	63.4	685

[a] $^{31}P\{^{1}H\}$ NMR: 121.65 MHz, $CDCl_3$, 298 K. [b] ppm. [c] Hz. [d] $^{31}P\{^{1}H\}$ NMR: 121.65 MHz, $CDCl_3$, 323 K.

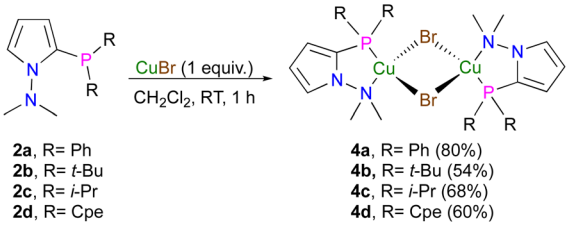

Scheme 2 Synthesis of dinuclear copper complexes **4a–d**.

PPh_3Se (Table 1, entry 5) indicating a stronger σ-donor behavior but less than the corresponding trialkylphosphines (Table 1, entries 6–8). In contrast, **3a** has the greatest J_{P-Se} value due to this best π-acceptor character.[19]

We prepared the air-stable complexes **4a–d** by reacting **2a–d** with CuBr in CH_2Cl_2. In all cases, a pale-yellow powder was isolated after recrystallization from diethyl ether (Scheme 2). As expected, in ^{1}H NMR, the proton signals were shifted at higher frequencies relative to the values assigned for free ligands. The same behavior occurs in ^{31}P NMR where the coordinated phosphine signals resonate at higher frequencies, due to the electron-withdrawing effect of the Cu atom. These spectroscopic data lead us to suggest that these ligands behave as bidentate donors (Table 2).

Table 2 ^{31}P NMR chemical shift (ppm) for [N,P] ligands based on pyrrole and their Cu(I) complexes[a]

Entry	Complex	$\delta^{31}P_{ligand}$	$\delta^{31}P_{complex}$	$\Delta\delta_{ligand/complex}$[b]
1	**4a**	−29.2	−34.3	−5.1
2	**4b**	1.5	11.5	10
3	**4c**	−17.6	−9.75	7.9
4	**4d**	−25.6	−17.5	7.7

[a] $^{31}P\{^1H\}$ NMR: 121.65 MHz, $CDCl_3$, 298 K. [b] ($\Delta\delta = \delta_{complex} - \delta_{ligand}$) ppm.

Suitable crystals for the X-ray analysis of these complexes were obtained from a solution of Et_2O. The solid-state molecular geometries of complexes **4a–d** were unequivocally confirmed by X-ray diffraction analysis (Fig. 2, 3 and S3, S4†). In a simple view, these complexes exhibit a tetrahedral geometry around the copper atom, with the [N,P] pyrrole-based ligands bonded in a κ^2-NP coordination mode. The complexes **4a–d** are dimers containing bromine atoms as a μ-bridge and have a five-membered metallacycle, in which the ligand has bite angles of P(1)–Cu(1)–N(2), 80.63°(6) for the complex **4a**, P(1)–Cu(1)–N(2), 84.97° (12) for **4b**, P(5)–Cu(5)–N(82), 81.81° (17) for **4c** and P(1)–Cu(1)–N(2), 84.56° (3) for **4d**.

All complexes have the expected tetra-coordinated environment around the copper metal center. To determine how closely these complexes could adopt a perfectly tetrahedral geometry Td ($\tau4$ = 1.0) or a perfectly trigonal pyramidal geometry C_{3v} ($\tau4$ = 0.85),[20] we calculated the angular structural parameter ($\tau4$) for **4a–d**, obtaining the following values: 0.77, 0.76, 0.73 and 0.81, respectively. From these data, we concluded that all complexes show highly distorted trigonal pyramidal geometries. Furthermore, the phosphine ligands and both bromides occupy the equatorial positions, whereas the dimethylamino group occupies the apical position in all complexes. The bond distances N(2)–Cu(1) 2.559(2) Å for complex **4a**, N(82)–Cu(5) 2.523(8) Å for complex **4c** and N(2)–Cu(1) 2.415(15) Å for **4d**, are slightly longer in comparison to that observed in complex **4b**, N(2)–Cu(1) 2.368(4) Å. This behavior suggests that for complexes **4a**, **4c** and **4d**, the phosphine group behaves as a strong σ-donor with a slight π-acceptor character, while in complex **4b**, the phosphine group only behaves as a strong σ-donor. The angles between Br(1)–Cu(1)–Br(1) 102.6° (3) for **4b** and Br(5)–Cu(5)–Br(6) 98.6° (4) for **4c** are narrower than those observed in complexes **4a** [Br(1)–Cu(1)–Br(1) 108.7° (2)] and **4d** [Br(2)–Cu(2)–Br(1) 109.8° (10)]. This fact prevents the Cu–Cu interaction observed in **4a** [Cu(1)–Cu(2) 2.844(10) Å] and **4d** [Cu(1)–Cu(2) 2.805(3)].

The UV/Vis absorption spectra of ligands **2a–d** and complexes **4a–d** acquired in CH_2Cl_2 are shown in Fig. 4. Both the

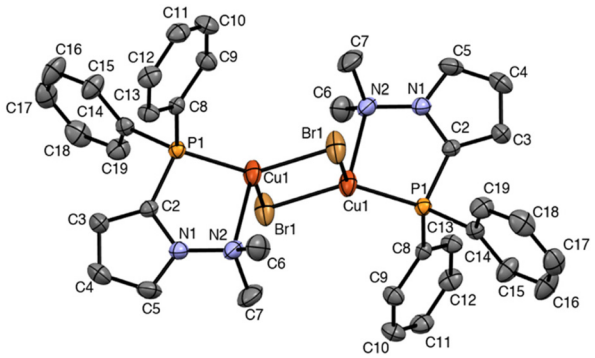

Fig. 2 ORTEP representation of ligand **4a**. Ellipsoids are shown at the 50% probability level. Selected bond lengths (Å) and bond angles (°): Br(1)–Cu(1), 2.4374(9); Br(1)–Cu(1), 2.4437(8); Cu(1)–P(1), 2.1910(9); Cu(1)–N(2), 2.559(2); P(1)–C(2), 1.808(3); P(1)–C(8), 1.822(2); P(1)–C(14), 1.836(2); N(1)–C(5), 1.371(3); N(1)–C(2), 1.373(3); N(1)–N(2), 1.422(3); N(2)–C(7), 1.480(4); N(2)–C(6), 1.481(4); Cu(1)–Br(1)–Cu(1), 71.28(2); P(1)–Cu(1)–Br(1), 126.82(3); P(1)–Cu(1)–Br(1), 122.39(3); Br(1)–Cu(1)–Br(1), 108.72(2); P(1)–Cu(1)–N(2), 80.63(6); Br(1)–Cu(1)–N(2), 100.31(6); Br(1)–Cu(1)–N(2), 105.38(6); 112.42(6); C(2)–P(1)–C(8), 105.70(11); C(2)–P(1)–C(14), 100.56(11); C(8)–P(1)–C(14), 103.72(11); C(2)–P(1)–Cu(1), 104.20(8); C(8)–P(1)–Cu(1), 116.57(8); C(14)–P(1)–Cu(1), 123.67(8); C(5)–N(1)–C(2), 110.3(2); C(5)–N(1)–N(2), 127.4(2); C(2)–N(1)–N(2), 122.3(2); N(1)–N(2)–C(7), 110.3(2); N(1)–N(2)–Cu(1), 105.55(14); N(1)–C(2)–P(1), 121.09(18).

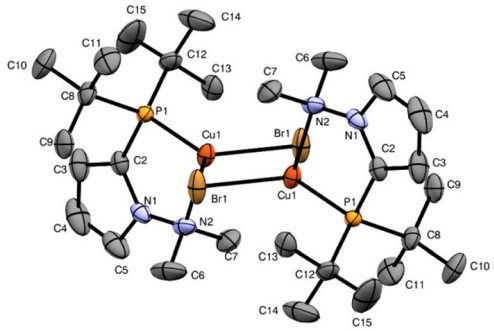

Fig. 3 ORTEP representation of ligand **4b**. Ellipsoids are shown at the 50% probability level. Selected bond lengths (Å) and bond angles (°): Br(1)–Cu(1), 2.4460(8); Br(1)–Cu(1), 2.4591(8); Cu(1)–P(1), 2.1888(13); Cu(1)–N(2), 2.368(4); P(1)–C(2), 1.809(5); P(1)–C(8), 1.880(5); P(1)–C(12), 1.886(6); N(1)–C(5), 1.350(7); N(1)–C(2), 1.388(7); N(1)–N(2), 1.412(6); N(2)–C(7), 1.462(7); N(2)–C(6), 1.475(8). Cu(1)–Br(1)–Cu(1), 77.35(3); P(1)–Cu(1)–N(2), 84.97(12); P(1)–Cu(1)–Br(1), 124.61(4); N(2)–Cu(1)–Br(1), 106.04(11); P(1)–Cu(1)–Br(1), 127.33(5); N(2)–Cu(1)–Br(1), 104.59(12); Br(1)–Cu(1)–Br(1), 102.65(3); C(2)–P(1)–C(8), 104.6(2); C(2)–P(1)–C(12), 103.9(3); C(8)–P(1)–C(12), 114.5(3); C(2)–P(1)–Cu(1), 103.22(19); C(8)–P(1)–Cu(1), 114.74(19); C(12)–P(1)–Cu(1), 114.0(2); C(5)–N(1)–C(2), 110.6(6).

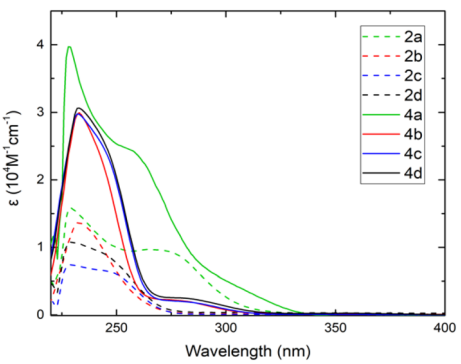

Fig. 4 UV–vis absorption spectra of **2a–d**, and **4a–d** in CH_2Cl_2 solution at room temperature.

complexes and the ligands exhibit similar intense and broad absorption bands (ε = 104 M^{-1} cm^{-1}) in the wavelength range from 225 to 285 nm, assigned to the allowed ligand-centered transitions (π–π* and n–π*) of **2a–d**. Complexes **4a–d** exhibit an intense absorption band in the 230–260 nm region, which is assigned to π–π* ligand-centered (LC) transitions of the N,P-ligand.[21] In the case of **4a**, we observed an additional absorption between ≈275 and ≈350 nm, which is attributed to metal-to-ligand charge-transfer (MLCT) transitions involving Cu(I) atoms and the ligand, while the complexes **4b–d** exhibit these transitions in the 265–290 nm region but with less intensity. We calculated the molar extinction coefficients (ε) for **4a** at 228 nm (ε = 43 090 M^{-1} cm^{-1}) and 265 nm (ε = 22 775 M^{-1} cm^{-1}), while the complexes **4b–d** showed a maximum absorption band located at 233 nm (ε = 32 434 M^{-1} cm^{-1}), (ε = 31 018 M^{-1} cm^{-1}), and (ε = 30 539 M^{-1} cm^{-1}), respectively.

In order to evaluate the catalytic performance of these copper complexes, we explored a 1,3-dipolar cycloaddition using the iminoester **5a** and *N*-phenyl maleimide **6** with 5% molar CuBr in the presence of Et_3N but only 19% yield of **7a** was obtained (Table 3, entry 1). To evaluate the effect of the ligand in the reaction, we used CuBr (5% mol) and the ligand **2a** (5.5% mol), achieving only 17% yield, suggesting that preformation of the catalytic complex must be essential to carry out the transformation (Table 3, entry 2). Thus, when the copper(I) salt was placed in the presence of ligand **2a** with a previous preformation of 30 min, the yield increased by 61%. This indicates that the use of the ligand is essential for stabilizing the intermediate copper species that are formed during the reaction (Table 3, entry 3). When the reaction was carried out with the copper catalytic precursor **4a**, we got a better result (75% yield), further confirming our assumption (Table 3, entry 4). Then, we tried to increase the yield by changing the copper precursor (Table 3, entries 5–8). The best result was obtained using $Cu(OTf)_2$ (Table 3, entry 7) in combination with ligand **2a**, reaching a 65% yield; however, the use of complex **4a** gave a slightly better yield (Table 3, entry 4). Regarding the organic base effect, we tested Et_3N and DIPEA; we determined that the nature of these two bases does not generate an evident change (Table 3, entries 4 and 11), but we need a stoichiometric amount of it, to have a higher yield (Table 3, entries 9–13).

Next, several experiments were carried out with different solvents, and the best result corresponds to EtOH reaching 95% yield (Table 3, entry 15). In general, using polar solvents such as AcOEt and acetonitrile, we obtained good yields (Table 3, entries 14 and 17). This behavior suggests that the dimeric complex **4a** is in equilibrium with its monomeric form

Table 3 Evaluation of catalytic conditions for the 1,3 dipolar cycloaddition reaction of imino esters of alanine **5a** and *N*-phenyl maleimide **6**[a]

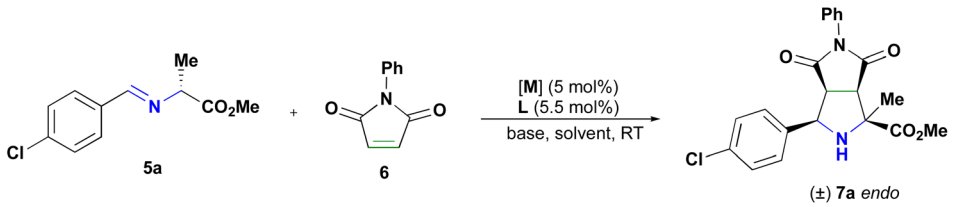

(±) **7a** *endo*

Entry	Copper precursor [M]	Ligand	Base (eq.)	Solvent	**7a** Yield[b] [%]	*endo*/*exo*
1	CuBr	—	Et_3N (1)	THF	19	—
2[c]	CuBr	**2a**	Et_3N (1)	THF	17	—
3[d]	CuBr	**2a**	Et_3N (1)	THF	61	—
4	**4a**	—	Et_3N (1)	THF	75	—
5[d]	Cu(OTf)	**2a**	Et_3N (1)	THF	54	—
6[d]	Cu(OAc)	**2a**	Et_3N (1)	THF	53	—
7[d]	$Cu(OTf)_2$	**2a**	Et_3N (1)	THF	65	—
8[d]	$Cu(OAc)_2$	**2a**	Et_3N (1)	THF	33	—
9	**4a**	—	Et_3N (0.5)	THF	65	—
10	**4a**	—	Et_3N (0.25)	THF	55	—
11	**4a**	—	DIPEA (1)	THF	73	—
12	**4a**	—	DIPEA (0.5)	THF	60	—
13	**4a**	—	DIPEA (0.25)	THF	54	—
14	**4a**	—	Et_3N (1)	AcOEt	83	—
15	**4a**	—	**Et_3N (1)**	**EtOH**	**95**	**Only *endo***
16	**4a**	—	Et_3N (1)	1,4-Dioxane	64	—
17	**4a**	—	Et_3N (1)	CH_3CN	56	—
18	**4a**	—	Et_3N (1)	Toluene	78	—
19	**4a**	—	Et_3N (1)	HFP[e]	18	—
20	**4b**	—	Et_3N (1)	EtOH	75	Only *endo*
21	**4c**	—	Et_3N (1)	EtOH	80	Only *endo*
22	**4d**	—	Et_3N (1)	EtOH	85	Only *endo*

[a] All reactions were performed with 1.0 mmol phenyl maleimide, 1.5 mmol imino ester **5a** and 2 mL of solvent at room temperature. [b] Isolated yield after SiO_2 column chromatography. [c] Without previous activation [Cu] and ligand. [d] Previous activation [Cu] and ligand 30 min. [e] HFP is 1,1,1,3,3,3-hexafluoro-2-propanol.

in solution, forming **4a′** (*vide infra*). Finally, we studied the Sigma donor effect on the phosphine group, and for this, we tested **4a–d** (Table 3, entries 15 and 20–22) in this cycloaddition reaction. All complexes catalyzed the reaction in good to excellent yields; the best result was obtained with **4a** (Table 3, entry 15). The *endo*/*exo* ratio diastereoselectivity in product **7a** was determined by ^{1}H NMR, and in all cases, only the *endo* adduct was observed (Table 3, entries 15 and 20–22).

The previous results allowed us to expand the scope of the reaction, obtaining pyrrolidines with substituents in position 2. This was done using imines derived from essential amino acids such as methionine and serine, in addition to those already reported derivatives of alanine and phenylglycine (see the ESI†). Once the imines **5a–i** were successfully obtained,[22] they were exposed to the best reaction conditions, furnishing in all cases the *endo*-adducts **7**, in good to excellent yields (Table 4, entries 1–5). This confirms that our methodology is effective for obtaining new pyrrolidines with different substituents at position 2 in a diastereoselective manner.

At this point, our interest focused on observing the behavior of the dinuclear complex **4a** in obtaining endo-selectivity when the imine had a different electronic contribution at the R^3 position. The results obtained had a pleasant trend in all cases, with yields ranging from moderate to good and only the *endo* adduct was observed (Table 4, entries 6–9).

The high endo-diastereoselectivity could be explained in two possible ways; a π interaction between the benzene ring in maleimide and the copper atom, or an N–Cu interaction between maleimide and the complex within the *endo* transition state. Subsequently, in order to gain insights into the origin of *endo* diastereoselectivity, we used *N*-methyl maleimide **8** as a dipolarophile, avoiding the possible Cu–π interaction. The reaction proceeded successfully in excellent yield (90%), furnishing only the *endo* diastereomer **9** (Scheme 3).

This finding suggests that the N–Cu interaction is responsible for the *endo* diastereoselectivity by anchoring the *endo* approximation between the azomethine ylide and the dipolarophile in the transition state.

Based on these results, we could propose the following reaction pathway to explain the *endo* product (Scheme 4). Initially, the metal complex **4a** undergoes a cleavage, induced by the solvent, forming the complex **4a′**. To probe this, we conducted a follow-up of the cleavage of **4a** in the presence of EtOH by ^{31}P-NMR (Fig. S152†). A similar behavior was observed in other copper(I) complexes.[23] We found that the addition of one drop of EtOH to a solution of **4a** in CD_2Cl_2 provokes a slight color change (colorless to pale-yellow) and the apparition of a new signal at −34.45 ppm. Likewise, we screened the UV-visible behavior of the solution of **4a** by the successive addition of EtOH, detecting a slight bathochromic shift (~10 nm) of the main absorption band placed at 238 nm (Fig. S153†). These results suggest the plausible cleavage of dimer **4a** in the presence of ethanol. Then, the imine is complexed in two stages (**A** and **B**); the base takes a proton, forming the catalytically active species **C**. In this step, the presence of a π-acceptor phosphine as **4a** (Table 1) in the catalytic precursor becomes critical to stabilize the formation of **C**. The follow-up of the reaction by ^{31}P NMR reveals a new signal at −32.77 ppm. The Cu(I)-coordinated iminoester initiates the catalytic cycle, interacting with the dipolarophile forming the transition state **D**, which is responsible for the formation of the *endo*-**7** product. Finally, we recorded a spectrum at the end of the reaction, detecting the presence of free ligand **2a** and its corresponding oxide (18.57 ppm).

DFT calculations were performed to find out if the proposed species **D** can explain the observed diasteroselectivity. The converged geometry of **D** also has a distorted trigonal pyramidal structure as in complex **4** but τ4 is significantly lower (0.59), due to the bite angle of the imine group. According to this calculation, the negative charge is delocalized between the imino group and the oxygen bonded to the copper, which could enhance its reactivity towards the maleimide group. Before the 3 + 2 addition, this charge distribution and the pyramidal structure of species **C** allow a strong intermolecular

Table 4 Scope of substituents on the azomethine ylide precursor in the 1–3 dipolar cycloaddition reaction[a]

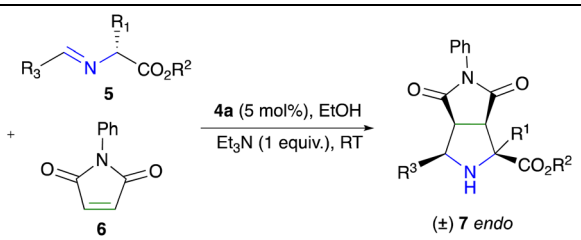

Entry	R^1	R^2	R^3	Product	Yield[b] [%]
1	Me	Et	*p*-Cl-C_6H_4	**7a**	95
2	Ph	Me	*p*-Cl-C_6H_4	**7b**	75
3	$CH_2CH_2SCH_3$	Et	*p*-Cl-C_6H_4	**7c**	85
4	CH_2OH	Me	*p*-Cl-C_6H_4	**7d**	80
5	Me	Et	*p*-F-C_6H_4	**7e**	74
6	Me	Et	Ferrocenyl	**7f**	56
7	Me	Et	2-Thienyl	**7g**	89
8	Me	Et	*p*-MeO-C_6H_4	**7h**	79
9	Me	Et	*p*-CF_3-C_6H_4	**7i**	85

[a] All reactions were performed with 1.0 mmol phenyl maleimide **6**, 1.5 mmol imino ester **5**, 1.0 mmol Et_3N, 2 mL of EtOH and 5%mol [Cu] **4a** at room temperature. [b] Isolated yield after SiO_2 column chromatography.

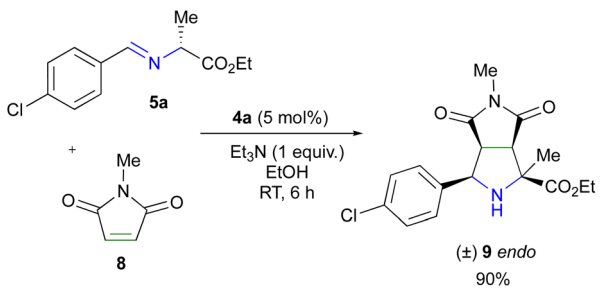

Scheme 3 Study of the origin of *endo* diastereoselectivity.

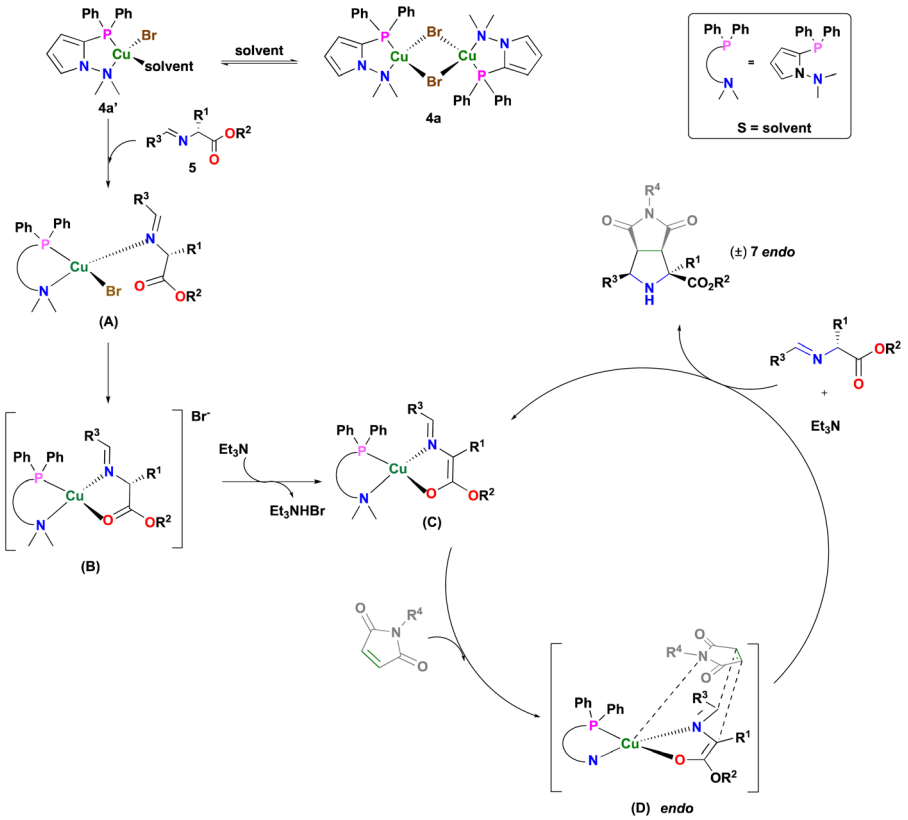

Scheme 4 Proposed pathway for the 1,3-cycloaddition catalyzed by complexes **4a'**.

interaction (18.1 kcal mol^{-1}) in an *endo* fashion between the π system of the imide and the base of the pyramid. The pyramid includes the imine, the metal center, and the substituents of phosphine.

The reduced density gradient (RDG) intermolecular isosurface that has been used to study non-covalent interactions,[24–26] shows that there are three main interactions between the complex **C** and the maleimide group (blue regions in Fig. 5a). The most prominent is the dipolar-π staking interaction between the reactive carbons. The second most important interaction occurs between the imide moiety and the Cu atom. The last relevant interaction is between the phenyl group of the maleimide and the groups of phosphine. Non-interactions between the carbonyl groups of maleimide and copper were observed as suggested by Hu *et al.*,[12j] and were responsible for the endo-selectivity.

This result was also confirmed from the bond paths that were obtained using the quantum theory of atoms in molecules (QTAIM); see the ESI.†

We searched for an energy minimum of the metal complex-maleimide dimer with an *exo* arrangement, but all the attempts ended in the *endo* geometry, which indicates that the imide preferably approaches species **C** with an *endo* orientation. After this approach, it is still possible to form an *exo* transition state (TS), but according to the calculation, this TS is significantly more energetic than the *endo* TS (8.1 kcal mol^{-1}, Fig. 5b). Moreover, the *endo* product is also less energetic than the *exo* product. Changing the phenyl group of the maleimide for a methyl group, as was performed experimentally does not change the energetic order of the *endo* and *exo* TS, which coincides with the experimental observations. However, the energy difference between these two TSs is reduced (4.4 kcal mol^{-1}, Fig. 5c), which confirms that the intermolecular interactions of the phenyl group are important but are not the only relevant ones. The calculations show that the pyramidal structure of the Cu complex allows the formation of several intermolecular interactions that are responsible for the endo-diasteroselectivity.

With these results in our hands, we decided to conduct a reaction using the nitrogen-free substrate **10** under the same reaction conditions standardized for this work (Scheme 5). The reaction was completed after one hour in an 88% yield, and the *endo*/*exo* ratio diastereoselectivity was determined by ^{1}H NMR, observing a 50 : 50 ratio of *endo*–*exo* adducts. These results agree with the mechanistic proposal since they put into evidence the role of the nitrogen atom included in the dipolarophile.

Comparing the catalytic performance of **4a** in this reaction with the results obtained for other catalytic systems (Table 5), we observed that our catalytic system exhibits a similar behavior to that of other catalytic systems involving [P,S]- or [N,N]-ligands. This catalytic system is robust and air-moisture stable.

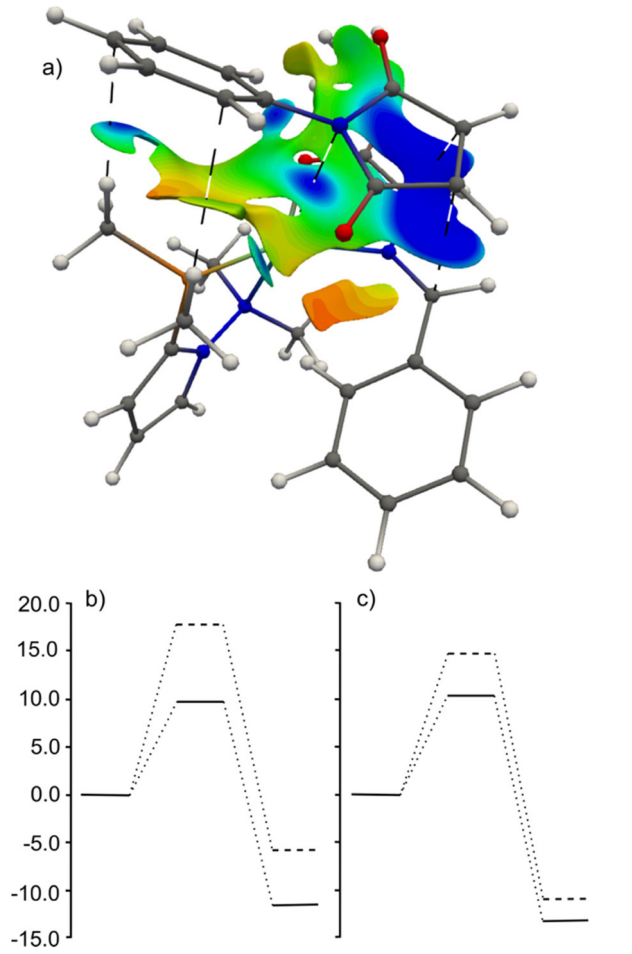

Fig. 5 (a) Intermolecular RDG surface of the interaction between species **C** and maleimide. The virial field [$V(r)$] is plotted over the isosurface. $V(r)$ color code: $\leq -5.0 \times 10^{-3}$ a.u. (dark blue), -2.5×10^{-3} a.u. (green) and 0.0 a.u. (red). *Endo* (solid line) and *exo* (dashed line) reaction paths of the [3 + 2] dipolar cycloaddition for (b) phenyl and (c) methyl maleimide. Relative energies in kcal mol^{-1}.

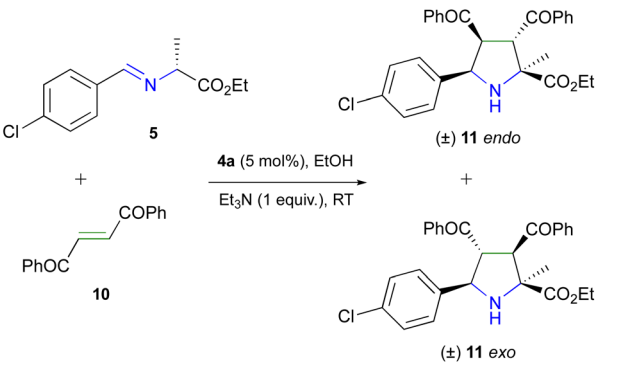

Scheme 5 Synthesis of pyrrolidines **11**.

Experimental

General considerations

All operations were carried out under an inert atmosphere of argon gas using standard Schlenk techniques. Column chromatography was performed using 70–230 mesh silica gel. All reagents and solvents were obtained from commercial suppliers and used without further purification. NMR spectra were obtained with a Bruker Avance III at 300 MHz for ^{1}H NMR, 75 MHz for $^{13}C\{^{1}H\}$ NMR, and 121 MHz for ^{31}P NMR using $CDCl_3$ as the solvent. Chemical shifts are expressed in ppm (δ), relative to TMS. All compounds were characterized by IR spectroscopy recorded on a PerkinElmer Spectrum 100 FT-IR equipped with an ATR accessory, and all data are expressed in wavenumbers (cm^{-1}). Melting points were obtained on a Melt-Temp II apparatus and were left uncorrected. The MS-FAB spectra were obtained on a JMS-SX102A using nitrobenzyl alcohol and polyethylene glycol matrices. MS-DART spectra were obtained on an AccuTOF JMS-T100LC; the values of the signals are expressed in mass/charge units (m/z).

UV-Vis absorption spectra were recorded using a Thermo Scientific Evolution 60S UV-visible spectrophotometer, using spectrophotometric grade CH_2Cl_2 solvent purchased from Sigma-Aldrich Co. and a 1 cm quartz cell.

Structure determination by X-ray crystallography

Suitable X-ray-quality crystals of **4a–d** were grown by slow evaporation of a mixture of diethyl ether/hexane at −5 °C, respectively. The crystals of each compound were mounted on a glass fiber at room temperature. The crystals of **4a–d** were then placed on a Bruker D8 Venture (**4a–b**) or APEX-II CCD (**4c–d**) with Mo-Kα radiation; the decay was negligible in all cases. Details of the crystallographic data collected for compounds **4a–d** are provided in Table 6. Systematic absences and intensity statistics were used in space group determinations. The structure was solved using direct methods.[27] Anisotropic structure refinements were achieved using the full matrix least-squares technique on all non-hydrogen atoms. All hydrogen atoms were placed in idealized positions based on hybridization, with isotropic thermal parameters fixed at 1.2 times the value of the attached atom. Structural solutions and refinements were performed using SHELXTL V6.10.[28] Crystallographic data for **4c** and **4d** are available in the CIF format in the ESI.† The X-ray crystallographic structures of compounds **4a–d** are available in the CCDC.

Theoretical methods

All geometry optimizations were performed in Gaussian 16[29] with the M06/def2-TZVP level of theory. A frequency calculation was performed for all the structures to confirm that the TS and the energy minimum have 1 or 0 imaginary frequencies, respectively. The obtained wave functions from these calculations were used to calculate all the density properties with the AIMALL software.[30] The RDG isosurface of the non-covalent interaction between species **D** and the maleimide moiety was plotted with the ParaView program. Over this surface, besides the $V(r)$ discussed in the main text, was also plotted the density multiplied by the sign of the second eigenvalue of its hessian (sign($\lambda 2$)ρ), which is the property that is usually used in the NCI method.[31] However, this plot does not show which are the most important interactions (see the ESI†).

Table 5 Catalytic performance of copper complexes in the synthesis of *endo*-adducts obtained by 1,3- dipolar cycloaddition between iminoesters and alkenes

Entry	Ligand	Conditions	*endo*-Adduct	Time	Examples	Ref.
1	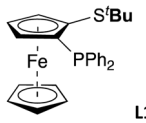 **L1**	$Cu(MeCN)_4ClO_4$ (3 mol%) (*R*)-**L1** (3 mol%) Et_3N (18%), CH_2Cl_2 4 Å MS, −10 °C	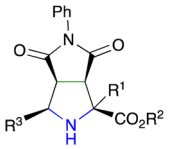 (1*S*,3*R*,3a*S*,6a*R*)-*endo*	15–60 min	6	12*m*
2	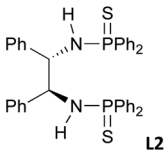 **L2**	$Cu(MeCN)_4ClO_4$ (5 mol%) **L2** (5.5 mol%)[a] ^{i}PrNEt (10 mol), CH_2Cl_2 −40 °C	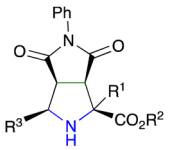 (1*S*,3*R*,3a*S*,6a*R*)-*endo*	24 h	10	12*l*
3	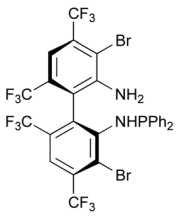 **L3**	$CuBF_4$ (3 mol%) **L3** (3 mol%)[a] Et_3N (15%), CH_2Cl_2 0 °C	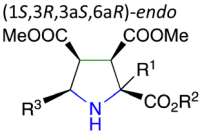 (2*R*,3*S*,4*R*,5*S*)-*endo*	10 min	13	12*k*
4	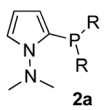 **2a**	**4a** (5 mol%)[b] Et_3N (1 eq.), EtOH, RT	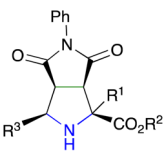 (±)-*endo*	0.5–1 h	10	This work

[a] Pre-formation of the copper complex *in situ*, 1 h. [b] Copper complex **4a** synthesized and isolated.

Table 6 Crystal data and structure refinement for compounds **4a–d**

Compound	**4a**	**4b**	**4c**	**4d**
Empirical formula	C_{36} H_{38} Br_2 Cu_2 N_4 P_2	$C_{28}H_{54}Br_2Cu_2N_4P_2$	C_{24} H_{46} Br_2 Cu_2 N_4 P_2	C_{32} H_{54} Br_2 Cu_2 N_4 P_2
Formula weight (g mol^{-1})	875.54	795.59	739.49	843.63
Crystal size (nm)	0.414 × 0.382 × 0.222	0.377 × 0.354 × 0.184	0.408 × 0.378 x0.336	0.405 × 0.362 × 0.238
Color	Colorless	Colorless	Colorless	Colorless
Crystal system	Triclinic	Monoclinic	orthorhombic	Monoclinic
Space group	$P\bar{1}$	$P2_1/c$	Pc	$P2_1/c$
a (Å)	8.817(3)	14.1029(8)	48.617(2)	8.7269(3)
b (Å)	9.727(3)	9.0827(4)	12.8598(5)	16.8301(7)
c (Å)	12.564(4)	15.0051(7)	15.4227(6)	24.7526(10)
α (°)	94.751(12)	90	90	90
β (°)	105.422(11)	108.427(2)	90	93.2040(10)
γ (°)	99.772(12)	90	90	90
V (Å^3)	1014.3(6)	1823.49(16)	9642.3(7)	3629.8(2)
Z	1	2	12	4
Temperature (K)	298	298	100	100
D_{calc} (g cm^{-3})	1.433	1.449	1.528	1.544
Number of collected reflections	25 914	20 959	116 095	48 837
Number of independent reflections (R_{int})	4839, R_{int} = 0.0655	5114, R_{int} = 0.0623	30 479, R_{int} = 0.0637	12 070, R_{int} = 0.036
Maximum and minimum transmission	0.4091 and 0.7460	0.5405 and 0.746	0.572 and 0.7462	0.6068 and 0.7464
Data/parameters	4839/210	20 959/180	30 479/1023	12 070/383
Final R indices	R = 0.0368	R = 0.0632	R = 0.0617	R = 0.0289
[$I > 2\sigma(I)$]	wR_2 = 0.0864	wR_2 = 0.1499	wR_2 = 0.1357	wR_2 = 0.0668
R indices (all data)	R = 0.0679, wR_2 = 0.076	R = 0.1278, wR_2 = 0.1277	R = 0.0744, wR_2 = 0.1312	R = 0.0403, wR_2 = 0.0636
GoF(F^2)	1.029	1.022	1.149	1.022
Absorption correction method	Multi-scan	Multi-scan	Multi-scan	Multi-scan
Clave	2295705	2295706	2295707	2295708

Moreover, recently it has been proved that sign $(\lambda 2)\rho$ is not appropriate for studying the strength of π–π interactions,[32] because of that we used $V(r)$ instead of essential experimental procedures/data.

Synthesis of ligands 2a–d

The synthesis of ligands **2a–d** was conducted following the procedures reported in the literature.[14,15]

Synthesis of complex 4a–d

In a 50 mL Schlenk flask was placed the corresponding ligand **2** (0.5 mmol, 1 equiv.), followed by the addition of CuBr (0.5 mmol, 1 equiv.). The flask was then purged with N_2, and anhydrous CH_2Cl_2 (5 mL) was added. The reaction mixture was stirred for approximately 1 hour at room temperature. Upon completion of the reaction, the solvent was removed under vacuum, leaving behind a white residue, which was then washed with hexane to obtain the pure complex **4**.

General procedure for the 1,3 dipolar cycloaddition reaction

To a solution of the appropriate imino ester (1.2 mmol) in 3.0 mL of EtOH were added 0.17 mL of Et_3N (1.2 mmol) and *N*-phenyl maleimide (174 mg, 1 mmol). Then, 0.03 mmol (27 mg) of **4a** were added under a nitrogen atmosphere. The reaction mixture was stirred at room temperature for 3 hours. Then, the reaction mixture was evaporated under vacuum and the crude was redissolved with 5 mL of CH_2Cl_2 and washed with H_2O (3 × 15 mL). The organic phase was dried with anhydrous sodium sulfate and then filtered through a pad of Celite and alumina, using 5.0 mL of CH_2Cl_2. Subsequently, the solvent was removed under reduced pressure. The crude was further purified through silica gel chromatography (eluent: 7 : 3 hexanes/EtOAc) to obtain the corresponding adducts.

Conclusions

In summary, we have developed a new family of Cu(I) dinuclear complexes based on [N,P]-pyrrole ligands. These complexes are air-stable dimers that contain bromine atoms as μ-bridges and exhibit a five-membered metallacycle with a highly distorted trigonal pyramidal geometry in all cases.

The developed catalytic system allows us to obtain substituted pyrrolidines with high endo-diastereoselectivity under mild conditions, with yields ranging from good to excellent. Likewise, theoretical experiments showed that the diastereoselectivity arises from a strong N–Cu interaction between the maleimide substrate and the copper catalytic species in the cycloaddition transition state, resulting in the formation of the *endo* adduct in all cases. The development of the chiral version of these ligands is in progress in our laboratories. In this way, the catalytic system can be used in the synthesis of natural and pharmaceutical products that require diastereoselective conditions with a high degree of reliability.

Conflicts of interest

There are no conflicts to declare.

Acknowledgements

The authors would like to acknowledge the technical assistance provided by M. Carmen García González, M. Paz Orta, Isabel Chávez, and César I. Sandoval Chávez and Diego Martínez Otero. We also thank the projects PAPIIT IN216323, and DGTIC (project LANCAD-UNAM-DGTIC-304) for the computer time. Miguel A. Alvarado-Castillo also thanks CONACYT for the Ph.D. grant.

References

1 For selected reviews on OLED uses see: (*a*) C. E. Hosecroft and E. C. Constable, *J. Mater. Chem. C*, 2022, **10**, 4456–4482; (*b*) V. K.-M. Au, *Energy Fuels*, 2021, **35**, 18982–18999; (*c*) H. Yersin, R. Czerwieniec, M. Z. Shafikov and A. F. Suleymanova, *ChemPhysChem*, 2017, **18**, 3508–3535.

2 For selected references see: (*a*) F. Doettinger, Y. Yang, M. Karnahl and S. Tschierli, *Inorg. Chem.*, 2023, **62**, 8166–8178; (*b*) F. Doettinger, M. Obermeir, V. Caliskanyürek, L. E. Burmeister, C. Kleeberg, M. Karnahl, M. Schwalbe and S. Tschierli, *ChemCatChem*, 2023, **15**, e202300452; (*c*) F. Sueyoshi, X. Zhang, K. Yamauchi and K. Sakai, *Angew. Chem., Int. Ed.*, 2023, **62**, e202217807; (*d*) B. Ma, Q. Xia, D. Wang, J.-K. Jin, Z. Li, Q.-J. Liang, M.-Y. Sun, D. Liu, L.-J. Liu, H.-X. Shu, J. Yang, D. Li and J. He, *Angew. Chem., Int. Ed.*, 2023, **62**, e202300233; (*e*) C. Dragonetti, M. Magni, A. Colombo, F. Fagnani, D. Roberto, F. Melchiorre, P. Biagni and S. Fantacci, *Dalton Trans.*, 2019, **48**, 9703–9711.

3 J.-B. Xie, S. Lin, S. Qiao and G. Li, *Org. Lett.*, 2016, **18**, 3926–3929.

4 A. Buchcic, A. Zawisza, S. Lésniak and M. Rachwalski, *Catalysts*, 2020, **10**, 971.

5 M. C. Schwarzer, A. Fujioka, T. Ishii, H. Ohmiya, S. Mori and M. Sawamura, *Chem. Sci.*, 2018, **9**, 3484–3493.

6 B. V. Rokade and P. J. Guiry, *J. Org. Chem.*, 2019, **84**, 5763–5772.

7 For selected reviews on 1,3-dipolar cycloadditions, see: (*a*) S. Dubey, A. Pal, S. Roy, S. Sasmal, A. Tamrakar, R. Jana and T. Das, *New J. Chem.*, 2023, **47**, 8997–9034; (*b*) S. V. Kumar and P. J. Guiry, *Chem. – Eur. J.*, 2023, **29**, e202300296; (*c*) J. Adrio and J. C. Carretero, *Chem. Commun.*, 2019, **55**, 11979–11991; (*d*) M. Ríos-Gutiérrez and L. R. Domingo, *Eur. J. Org. Chem.*, 2019, 267–282; (*e*) J. Adrio and J. C. Carretero, *Chem. Commun.*, 2011, **47**, 6784–6794; (*f*) A. Cózar and F. P. Cossío, *Phys. Chem. Chem. Phys.*, 2011, **13**, 10858–10868.

8 (*a*) Z.-H. Wang, J.-H. Liu, Y.-P. Zhang, J.-Q. Zhao, Y. You, M.-Q. Zhou, W.-Y. Han and W.-C. Yuan, *Org. Lett.*, 2022, **24**, 4052–4057; (*b*) S. Furuya, K. Kanemoto and S.-I. Fukuzawa,

Chem. – Asian J., 2022, **17**, e202200239; (*c*) A. G. Taha, E. E. Elboray, Y. Kobayashi, T. Furuta, H. H. Abas-Temirek and M. F. Aly, *J. Org. Chem.*, 2021, **86**, 547–558; (*d*) W.-R. Zhu, Q. Su, N. Lin, Q. Chen, Z.-W. Zhang, J. Weng and G. Lu, *Org. Chem. Front.*, 2020, **7**, 3452–3458; (*e*) J. Otero-Fraga, S. Suárez-Pantiga, M. Montesinos-Magraner, D. Rhein and A. Mendoza, *Angew. Chem., Int. Ed.*, 2017, **56**, 12962–12966.

9 (*a*) S. V. Kumar and P. J. Guiry, *Angew. Chem., Int. Ed.*, 2022, **61**, e202205516; (*b*) Y. Yi, Y.-Z. Hua, H.-J. Lu, L. T. Liu and M.-C. Wang, *Org. Lett.*, 2020, **22**, 2527–2531; (*c*) I. N. Chaithanya Kiran, K. Fujita, S. Tanaka and M. Kitamura, *ChemCatChem*, 2020, **12**, 5613–5617.

10 Z. T. Gugkaeva, M. V. Panova, A. F. Smol'yakov, M. G. Medvedev, A. T. Tsaloev, I. A. Godovikov, V. I. Maleev and V. A. Larionov, *Adv. Synth. Catal.*, 2022, **364**, 2395–2402.

11 (*a*) Q. Hou, Y. You, X. Song, Y. Wang, K. Chen and H. Wang, *Catalysts*, 2020, **10**, 28; (*b*) Y.-P. Zhang, Y. You, J.-Q. Zhao, X.-J. Zhou, X.-M. Zhang, X.-Y. Xu and W.-C. Yuan, *Org. Chem. Front.*, 2019, **6**, 1879–1884; (*c*) M. Zhi, Z. Gan, R. Ma, H. Cui, E.-Q. Li, Z. Duan and F. Mathey, *Org. Lett.*, 2019, **21**, 3210–3213; (*d*) A. Cayuelas, O. Larranaga, V. Selva, C. Nájera, T. Akiyama, J. M. Sansano, A. Cozar, J. I. Miranda and F. P. Cossio, *Chem. – Eur. J.*, 2018, **24**, 8092–8097; (*e*) X. Zheng, Q. Deng, Q. Hou, K. Zhang, P. Wen, S. Hu and H. Wang, *Synthesis*, 2018, **50**, 2347–2358.

12 (*a*) B.-R. Wang, Y.-B. Li, Q. Zhang, D. Gao, P. Tian, Q. Li and L. Yin, *Nat. Chem.*, 2023, **14**, 4688; (*b*) X. Chang, X.-T. Liu, F. Li, Y. Yang, L. W. Chung and C.-J. Wang, *Chem. Sci.*, 2023, **14**, 5460–5469; (*c*) X. Xu, L. Bao, L. Ran, Z. Yang, D. Yan, C.-J. Wang and H. Teng, *Chem. Sci.*, 2022, **13**, 1398–1407; (*d*) H. Cui, K. Li, Y. Wang, M. Song, C. Wang, D. Wei, E.-Q. Li, Z. Duan and F. Mathey, *Org. Biomol. Chem.*, 2022, **18**, 3740–3746; (*e*) H. Deng, T. T. Liu, Z. D. Ding, W. L. Yang, Y. Luo and W. P. Deng, *Org. Chem. Front.*, 2020, **7**, 3247–3252; (*f*) S. N. Greszler, G. Zhao, M. Buchman, X. B. Searle, B. Liu and E. A. Voight, *J. Org. Chem.*, 2020, **85**(11), 7620–7632; (*g*) G. S. Caleffi, O. Larrañaga, M. Ferrándiz-Sapewras, P. R. R. Costa, C. Nájera, A. Cozar, F. P. Cossío and J. M. Sansano, *J. Org. Chem.*, 2019, **84**, 10593–10605; (*h*) H. Deng, R. Jia, W. L. Yang, Z. Yu and W. P. Deng, *Chem. Commun.*, 2019, **55**, 7346–7349; (*i*) F. Tian, F.-S. He, H. Deng, W.-L. Yang and W.-P. Deng, *Org. Lett.*, 2018, **20**, 3838–3842; (*j*) F.-Z. Han, S.-B. Yu, C. Zhang and X.-P. Hu, *Tetrahedron*, 2016, **72**, 2616–2622; (*k*) C.-J. Wang, G. Liang, Z.-Y. Xue and F. Gao, *J. Am. Chem. Soc.*, 2008, **130**, 17250–17251; (*l*) M. Shi and J. W. Shi, *Tetrahedron: Asymmetry*, 2007, **18**, 645–650; (*m*) S. Cabrera, R. Gómez Arrayás and J. C. Carretero, *J. Am. Chem. Soc.*, 2005, **127**, 16394–16395.

13 (*a*) F. Cheng, S. J. Kalita, Z.-N. Zhao, X. Yang, Y. Zhao, U. Schneider, N. Shibat and Y.-Y. Huang, *Angew. Chem., Int. Ed.*, 2019, **58**, 16637–16643; (*b*) I. Rivilla, A. Cózar, T. Schäfer, F. J. Hernandez, A. M. Bittner, A. Eleta-Lopez, A. Aboudzadeh, J. I. Dsantos, J. I. Miranda and F. Cossío, *Chem. Sci.*, 2017, **8**, 7038–7043; (*c*) F.-F. Tang, W.-L. Yang, X. Yu and W.-P. Deng, *Catal. Sci. Technol.*, 2015, **5**, 3568–3575; (*d*) L. M. Castelló, C. Nájera, J. M. Sansano, O. Larrañaga, A. Cózar and F. P. Cossío, *Synthesis*, 2015, **47**, 934–943.

14 J. V. Súarez-Meneses, E. Bonilla-Reyes, E. A. Blé-González, M. C. Ortega-Alfaro, R. A. Toscano, A. Cordero-Vargas and J. G. López-Cortés, *Tetrahedron*, 2014, **70**, 1422–1430.

15 (*a*) J. V. Suarez-Meneses, A. Oukhrib, M. Gouygou, M. Urrutigoïty, J.-C. Daran, A. Cordero-Vargas, M. C. Ortega-Alfaro and J. G. López-Cortés, *Dalton Trans.*, 2016, **23**, 9621–9630; (*b*) S. Cortés-Mendoza, D. Adamczyk, J. Badillo-Gómez, M. Urrutigoity, M. C. Ortega-Alfaro and J.-G. López-Cortés, *Adv. Synth. Catal.*, 2022, **364**, 2837–2845.

16 E. P. Sánchez-Rodríguez, S. Cortés-Mendoza, J.-C. Daran, M. C. Ortega-Alfaro, J. G. López-Cortés and M. Gouygou, *Appl. Organomet. Chem.*, 2020, **34**, e5709.

17 E. P. Sánchez-Rodríguez, A. J. Fragoso-Medina, E. Ramírez-Meneses, M. Gouygou, M. C. Ortega-Alfaro and J. G. López-Cortés, *Catal. Commun.*, 2018, **115**, 49–54.

18 Z. L. Niemeyer, A. Milo, D. P. Hickey and M. S. Sigman, *Nat. Chem.*, 2016, **8**, 610–617.

19 W. D. Allen and B. F. Taylor, *J. Chem. Soc., Dalton Trans.*, 1982, 51–54.

20 (*a*) A. W. Addison and T. Nageswara Rao, *J. Chem. Soc., Dalton Trans.*, 1984, 1349–1356; (*b*) S. R. Harutyunyan, F. López, W. R. Browne, A. Correa, D. Peña, R. Badorrey, A. Meetsma, A. J. Minnaard and B. L. Feringa, *J. Am. Chem. Soc.*, 2006, **128**, 9103–9118.

21 (*a*) R. Czerwieniec, K. Kowalski and H. Yersin, *Dalton Trans.*, 2013, **42**, 9826–9830; (*b*) M. Knorn, T. Rawner, R. Czerwieniec and O. Reiser, *ACS Catal.*, 2015, **5**, 5186–5193.

22 S. Xu, Z.-M. Zhang, B. Xu, B. Liu, Y. Liu and J. Zhang, *J. Am. Chem. Soc.*, 2018, **140**, 2272–2283.

23 W. Liang, K. Nakajima, K. Sakata and Y. Nishibayashi, *Angew. Chem., Int. Ed.*, 2019, **58**, 1168–1173.

24 E. R. Johnson, S. Keinan, P. Mori-Sánchez, J. Contreras-García, A. J. Cohen and W. Yang, *J. Am. Chem. Soc.*, 2010, **132**, 6498–6506.

25 G. Saleh, C. Gatti and L. Lo Presti, *Comput. Theor. Chem.*, 2015, **1053**, 53–59.

26 Y. Cornaton and J.-P. Djukic, *Acc. Chem. Res.*, 2021, **54**, 3828–3840.

27 A. Altomare, G. Cascarano, C. Giacovazzo, A. Guagliardi, M. C. Burla, G. Polidori and M. Canalli, *J. Appl. Crystallogr.*, 1994, **27**, 435.

28 G. M. Sheldrick, *Acta Crystallogr., Sect. A: Found. Crystallogr.*, 2008, **64**, 112.

29 M. J. Frisch, G. W. Trucks, H. B. Schlegel, G. E. Scuseria, M. A. Robb, J. R. Cheeseman, G. Scalmani, V. Barone, G. A. Petersson, H. Nakatsuji, X. Li, M. Caricato, A. V. Marenich, J. Bloino, B. G. Janesko, R. Gomperts, B. Mennucci, H. P. Hratchian, J. V. Ortiz, A. F. Izmaylov, J. L. Sonnenberg, D. Williams-Young, F. Ding, F. Lipparini,

F. Egidi, J. Goings, B. Peng, A. Petrone, T. Henderson, D. Ranasinghe, V. G. Zakrzewski, J. Gao, N. Rega, G. Zheng, W. Liang, M. Hada, M. Ehara, K. Toyota, R. Fukuda, J. Hasegawa, M. Ishida, T. Nakajima, Y. Honda, O. Kitao, H. Nakai, T. Vreven, K. Throssell, J. A. Montgomery Jr., J. E. Peralta, F. Ogliaro, M. J. Bearpark, J. J. Heyd, E. N. Brothers, K. N. Kudin, V. N. Staroverov, T. A. Keith, R. Kobayashi, J. Normand, K. Raghavachari, A. P. Rendell, J. C. Burant, S. S. Iyengar, J. Tomasi, M. Cossi, J. M. Millam, M. Klene, C. Adamo, R. Cammi, J. W. Ochterski, R. L. Martin, K. Morokuma, O. Farkas, J. B. Foresman and D. J. Fox, *Gaussian 16 Revision B.01*, Gaussian Inc., Wallingford, CT, 2016.

30 T. A. Keith, *AIMAll 2019, TK Gristmill Software*, Overland Park KS, USA, **aim.tkgristmill.com**.

31 E. R. Johnson, S. Keinan, P. Mori-Sánchez, J. Contreras-García, A. J. Cohen and W. Yang, *J. Am. Chem. Soc.*, 2010, **132**, 6498–6506.

32 D. Morales-Pumarino and J. E. Barquera-Lozada, *Int. J. Quantum Chem.*, 2023, **123**, e27051.